Effect of pressure on the magnetic properties of (Co0.5Fe0.5)5GeTe2

PAPER • **OPEN ACCESS**

Effect of pressure on the magnetic properties of $(Co_{0.5}Fe_{0.5})_5GeTe_2$

To cite this article: Tamás Prok *et al* 2026 *2D Mater.* **13** 035031

2D Materials

OPEN ACCESS

RECEIVED
9 June 2026

REVISED
16 July 2026

ACCEPTED FOR PUBLICATION
24 August 2026

PUBLISHED
7 September 2026

PAPER

Effect of pressure on the magnetic properties of $(Co_{0.5}Fe_{0.5})_5GeTe_2$

Tamás Prok[1,2,3], **Zoltán Kovács-Krausz**[1,2], **Harvey Stanfield**[4], **Bing Zhao**[5], **Michael Leonárd Morgan**[1], **Bálint Fülöp**[1], **Marcos H D Guimarães**[3], **Ivan J Vera-Marun**[4], **Saroj Prasad Dash**[5], **Szabolcs Csonka**[1,6,7], **Péter Makk**[1,2,*] and **Endre Tóvári**[1,2,*]

1 Department of Physics, Institute of Physics, Budapest University of Technology and Economics, Műegyetem rkp. 3., H-1111 Budapest, Hungary
2 MTA-BME Correlated van der Waals Structures Momentum Research Group, Műegyetem rkp. 3., H-1111 Budapest, Hungary
3 Zernike Institute for Advanced Materials, University of Groningen, Groningen, The Netherlands
4 Department of Physics and Astronomy, University of Manchester, Manchester M13 9PL, United Kingdom
5 Department of Microtechnology and Nanoscience, Chalmers University of Technology, SE-41296, Göteborg, Sweden
6 Department of Physics and Astronomy, University of Manchester, Manchester M13 9PL, United Kingdom
7 HUN-REN Centre for Energy Research, Institute of Technical Physics and Materials Science, Konkoly Thege Miklós út 29-33, 1121 Budapest, Hungary
* Authors to whom any correspondence should be addressed.

E-mail: makk.peter@ttk.bme.hu and tovari.endre@ttk.bme.hu

Keywords: van der Waals, antiferromagnet, magnetoresistance, hydrostatic pressure, anomalous Hall effect

Supplementary material for this article is available online

Abstract

Cobalt-doped Fe_5GeTe_2 possesses a rich magnetic phase diagram as a function of Co concentration. The nature of magnetic order in $(Co_{0.5}Fe_{0.5})_5GeTe_2$ is especially interesting, as it has been shown to exhibit ferromagnetic order, A-type antiferromagnetic (AFM) order, or potentially both at the same time. Here we present magnetoresistance measurements on AFM $(Co_{0.5}Fe_{0.5})_5GeTe_2$ at a series of pressures and extract the anisotropy and interlayer exchange fields using the two-sublattice model. We show a 50% increase of the interlayer exchange at 2 GPa, highlighting the sensitivity of magnetic properties to interlayer distance. In addition, we find that the sharp hysteretic transitions observed within the AFM state can be qualitatively described by a linear chain model, which suggests an even–odd effect as a function of layer number instead of a coexisting ferromagnetic phase.

1. Introduction

For spintronics applications, antiferromagnetic (AFM) materials possess multiple advantages compared to ferromagnets (FM). They exhibit negligible stray fields, are not sensitive to magnetic perturbations, and their internal spin dynamics are significantly faster [1, 2]. Moreover, they demonstrate potential in memory applications due to a large magnetoresistance, without requiring the fabrication of a multilayer tunnel junction device [3, 4]. Two-dimensional (2D) magnets are especially intriguing as they show a wide variety of magnetic ordering down to the monolayer thickness, and may be controlled by electric fields, current, or other means [5–8]. Due to their novel properties, atomic thickness, and impurity-free interfaces, 2D heterostructures built of magnetic and nonmagnetic layers offer new opportunities for the design of future spintronic devices [9–14].

Among 2D magnets, Fe_3GeTe_2 and Fe_3GaTe_2 have been shown to exhibit a moderate stability in air, a Curie temperature T_C approaching or exceeding room temperature, and they have a strong perpendicular magnetic anisotropy (PMA) relative to the molecular plane [15–17]. Their magnetic properties are highly sensitive to the composition, for example, increasing the Fe content can increase T_C on the order of a hundred Kelvins as shown in Fe_5GeTe_2 [18, 19]. Moreover, by substituting Fe with Co in Fe_5GeTe_2, the magnetic order can change drastically. Defining the Co concentration x as $(Co_xFe_{1-x})_5GeTe_2$ (CFGT for short), for approximately $x = 0.1 - 0.3$ the FM easy direction is in the *ab* plane [20–22]. In contrast, in

the $x = 0.4 - 0.5$ range, CFGT is an A-type antiferromagnet, i.e. magnetic moments in each molecular layer are ferromagnetically coupled, but the magnetization of neighboring layers is opposite, as depicted in figure 1(a). For these Co concentrations, PMA is recovered and the Néel temperature T_N ranges between approximately 300 and 430 K [20, 21, 23, 24]. However, a FM state has also been observed at $x = 0.5$ [25, 26], and it is also predicted to be present at $x = 0.6$ [21]. Moreover, coexisting AFM and FM order has been reported based on hysteretic features inside the AFM phase [23, 24]. The changes with increasing x have been tied to transitions from ABC to AA to AA' stacking [21, 25], although it is unclear why both FM and AFM states are possible around 50% Co substitution of Fe.

Here we show that the magnetic characteristics of CFGT can be actively tuned by another control knob: the interlayer distance via pressure [27]. Hydrostatic pressure has been shown to induce changes in stacking and magnetic order [28, 29]. We performed magnetoresistance measurements on multiple $(Co_{0.5}Fe_{0.5})_5GeTe_2$ samples and monitored their magnetic properties via the anomalous Hall effect (AHE) [30]. We have found that the AFM interlayer coupling is enhanced by 50% by a pressure p of 2 GPa. In addition, we propose that the hysteresis loops observed within the AFM phase can be explained by the behavior of the surface layers instead of the presence of a bulk FM order.

2. Methods

Single crystals of $(Co_{0.5}Fe_{0.5})_5GeTe_2$, grown by chemical vapor transport, were obtained from HQ Graphene. A scanning transmission electron microscope image is shown in figure 1(a), further characterization can be found in ref. [24]. We prepared 10–90 nm thick flakes by exfoliation onto SiO_2 substrates. Their thickness was measured by atomic force microscopy. Chromium/gold leads were deposited via standard electron beam lithography after cleaning the surface of the contact areas by argon-milling.

Figure 1(b) shows a photo of sample A, an approximately 90 nm-thick flake, and also illustrates the measurement geometry. We studied the Hall resistance R_{xy} of CFGT samples as a function of an applied out-of-plane magnetic field H at a series of temperatures T and hydrostatic pressures p up to 2 GPa. To apply pressure the samples were placed into a pressure cell which was filled with kerosene [27] during all of the measurements. The electrical measurements were performed in a variable temperature insert, using lock-in amplifiers and differential amplifiers. The current used for the resistance measurements was generally $I_{rms} = 10\,\mu$A at $f = 132.43$ Hz.

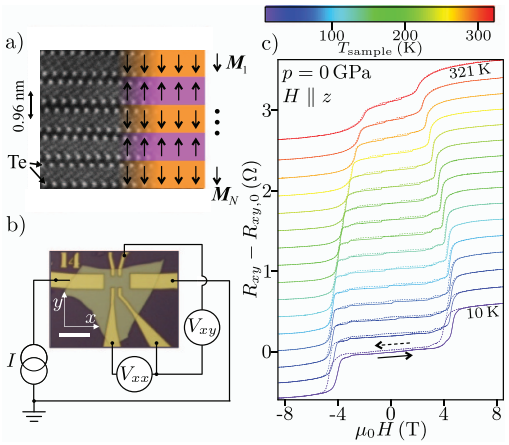

Figure 1. (a) Scanning transmission electron microscope image of a CFGT crystal. The brightest spots are Te atoms. The alternating magnetization in neighboring layers in the AFM state is illustrated. The thickness of a molecular layer and its magnetization are indicated. (b) Optical image of 90 nm-thick sample A and a diagram of the measurement setup. The scale bar is 10 μm. (c) The Hall resistance of the sample at a series of selected temperatures. Solid (dotted) lines indicate data for up (down) sweeps of the field. A zero-field value $R_{xy,0}$, which is a result of the mixing of a longitudinal voltage drop, has been removed. The curves are plotted with offsets that are proportional to T.

3. Results

The Hall resistance of sample A at ambient pressure is shown in figure 1(c) from approximately 10 K up to above room temperature, after removal of a zero-field offset $R_{xy,0}$. All R_{xy} curves show step-like features that are symmetrical around $H = 0$. These are characteristic of an antiferromagnet with an approximately out-of-plane easy axis [1, 20, 23, 24, 31] where the behavior of the out-of-plane component of the magnetization $\boldsymbol{M}$ is reflected in R_{xy} via the AHE. A step during increasing $|H|$ corresponds to a first order phase transition from the AFM state towards the fully polarized FM phase. As we show further below, this is a spin flop (SF) transition in which the AFM state switches to a canted AFM (cAFM) state, and denote the corresponding field by H_{SF}. At high fields, R_{xy} appears to saturate, over an approximately linear background due to the conventional Hall effect (CHE). At most temperatures, the hysteresis between up- and down-sweeps of H is negligible at the SF transition, and only becomes clearer below ~ 50 K.

Another interesting feature of the data on sample A is a pair of small rectangular hysteresis loops at most T. As illustrated in figure 1(c) and magnified in figure 4(b), they are observable within the AFM phase ($|H| < H_{SF}$) even above room temperature. Each loop can be characterized by a pair of coercive fields with the same sign, and therefore have a negligible remanence at zero field, similarly to certain samples in ref. [23]. The exception is below 100 K, where the shift

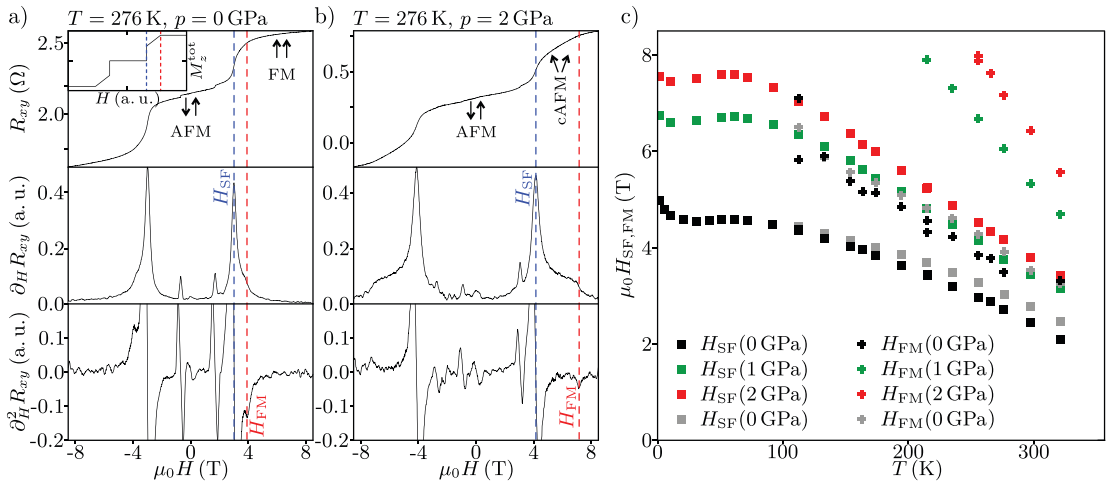

Figure 2. (a) and (b) Examples of the raw Hall data and its derivatives on sample A at 276 K as a function of increasing H at $p =$ 0 and 2 GPa, respectively. The vertical blue and red lines mark the H_{SF} and H_{FM} fields, respectively. Arrows illustrate the AFM, canted AFM and FM phases. The peaks in the derivatives within the AFM phase are due to the steps of the small hystereses. Inset: simulation of the total out-of-plane magnetization using the two-sublattice model. (c) The values of the H_{SF} (solid squares) and the H_{FM} (crosses) fields as a function of T at different pressures.

of the coercive fields leads to an overlap of the hysteresis loops and a finite remanence.

We extracted H_{SF} by identifying sharp peaks in the first derivative $\partial R_{xy}/\partial H$ as shown in figure 2(a) for an up-sweep of H. At low temperature where the SF transition is hysteretic, we averaged the H_{SF} of up and down sweeps. The results are plotted in figure 2(c) as solid black squares as a function of temperature. $\mu_0 H_{SF}$ decreases from approximately 5 to ~ 2 T between 1.5 and 320 K, which likely reflects the decrease of the absolute layer magnetization with increasing T. Under applied pressures up to $p =$ 2 GPa, the magnetoresistance curves are qualitatively similar to those taken at $p = 0$ GPa, as illustrated in figure 2(b). The obtained H_{SF}, plotted in figure 2(c) as a function of temperature for all pressures with solid squares, show similar trends with T, while we observe a monotonic increase in H_{SF} with p. The measurements performed after the release of pressure are shown in gray, and closely match the values before applying pressure (black). All datasets suggest that the Néel temperature is well above 350 K, in accordance with ref. [24].

We have investigated further CFGT samples and obtained similar results regarding the main features of the R_{xy} curves. Most data shown in the main text were measured on sample A unless stated otherwise. For an overview of all measurements, we refer to the Supplementary Information (SI) section 1.

4. Discussion

In the following, we show a framework that describes the dominant features of the magnetoresistance of CFGT, and reveal a giant tunability of the model parameters with pressure. Then we turn to the peculiar fine structure of the R_{xy} curves, i.e. the small hysteresis loops within the AFM phase, taken on several samples. We demonstrate that the model serves as a good foundation to explain the details of the magnetic behavior without invoking a simultaneous FM order.

Here we examine the nature of the magnetic phase transition at H_{SF}. Since H is approximately aligned with the easy axis [24], the step is either a spin flip transition directly from the AFM to the FM phase, or a SF transition to an intermediate, cAFM state where the layer magnetizations are not collinear [1]. In the latter case, the net magnetization jumps to a finite value at H_{SF}, followed by a continuous change during the cAFM phase until the onset of the FM phase, as shown in the inset of figure 2(a). This point is denoted by H_{FM} and is accompanied by a dip in the second derivative, $\partial^2 R_{xy}/\partial H^2$, while it is absent in the spin flip case. Such a feature is clearly visible in the second derivative of the data as highlighted by the red dashed line in figure 2(b), confirming the presence of the cAFM state at 2 GPa. A dip of the second derivative is also present at 0 GPa (figure 2(a)), although it is less distinct, as its distance to H_{SF} is four times smaller. These results show that pressure stabilizes the cAFM phase compared to the ambient state. The obtained H_{FM} fields are plotted in figure 2(c) as crosses. We note that we could only extract H_{FM} for a limited range in temperature since it increases with decreasing T and goes above our experimental limitations ($\mu_0|H| = 8.5$ T).

In order to gain further insight into the main magnetoresistance features and the role of pressure, we turn to the two-sublattice model of A-type AFMs [32]. This assumes that each layer has uniform, saturated magnetization and that the surface layers' magnetization is negligible compared to the bulk. This

applies to sample A, where the layer number N, using a layer thickness of 0.96 nm (see also figure 1(a)) [20, 25], is around 94. Therefore, every second layer can be considered equivalent in the AFM phase, and the system can be described as two coupled sublattices. The directions of the sublattice magnetizations $\boldsymbol{M}_{1,2}$ can be determined by minimizing the following energy functional:

$$f = J\boldsymbol{M}_1 \cdot \boldsymbol{M}_2 - \sum_{i=1,2} \left(\frac{K}{2} M_{iz}^2 + \boldsymbol{H} \cdot \boldsymbol{M}_i \right) \qquad (1)$$

where the signed bracket is essentially the Stoner-Wohlfarth energy [33]. Here, units of Am^{-1} are used for the interlayer exchange $J > 0$, the anisotropy $K > 0$ and the applied field $\boldsymbol{H}$, while $\boldsymbol{M}_{1,2}$ are dimensionless unit vectors. We have calculated the phase diagram of the system by identifying the lowest-energy stable solution (global minimum) at any point on the $H/2J, K/J$ plane. It is plotted as a colormap of the z component M_z of the total magnetization ($\boldsymbol{M} = \boldsymbol{M}_1 + \boldsymbol{M}_2$) in figure 3(a). The model predicts that if $K < J$, we may observe the AFM, cAFM, then FM phases as H is increased from 0, with distinct transitions at H_{SF} and H_{FM}. We can express the phase transition fields defined above as

$$H_{\mathrm{SF}} = \sqrt{K(2J-K)}, \qquad (2a)$$

$$H_{\mathrm{FM}} = 2J - K. \qquad (2b)$$

We plot the theoretical H_{SF} and H_{FM} in figure 3(a) after rescaling with $2J$ as black and white dashed lines, respectively, which clearly delineate the three phases. If $K > J$, the canted state is no longer a global energy minimum, leading to a spin-flip transition at $H_{\mathrm{SF}} = H_{\mathrm{FM}} = J$. Based on equations (2a), (2b) and the experimental values of $H_{\mathrm{SF}}, H_{\mathrm{FM}}$ in figure 2(c), we calculated the effective temperature-dependent parameters $K(T), J(T)$ and plotted them in figure 3(b). In general, the anisotropy K is independent of pressure, while the interlayer exchange J increases by as much as 50% with p, likely due to the decreased distance between the layers as in ref. [34].

The effective K and J decrease as T is increased, which may be attributed to the reduction of the actual magnetization of the layers. We can separate the latter into an unknown, dimensionless $M(T)$ function [35] and substitute $M(T)\boldsymbol{M}_i$ into equation (1) in place of $\boldsymbol{M}_i$. As a result, we can rewrite equations (2a), (2b) to describe the observed temperature-dependent transition fields as follows:

$$H_{\mathrm{SF}}(T) = M(T)\sqrt{K(2J-K)}, \qquad (3a)$$

$$H_{\mathrm{FM}}(T) = M(T)(2J-K). \qquad (3b)$$

Now K, J are independent of temperature. While individually they cannot be determined from experiments, a dimensionless parameter can be defined from the ratio of the spin-flop and saturation fields. In this picture $H_{\mathrm{SF}}(T)/H_{\mathrm{FM}}(T) = \sqrt{K/(2J-K)}$ is

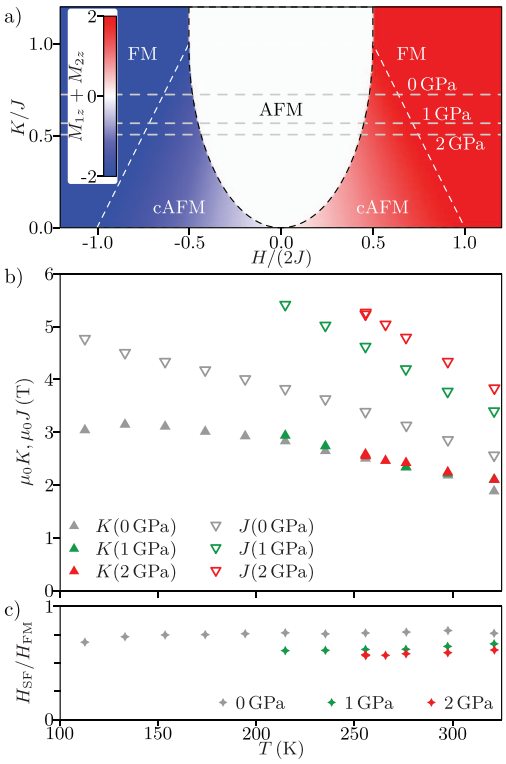

Figure 3. (a) Phase diagram of the two-sublattice system according to the numerically calculated global minimum of equation (1). The black dashed line shows the analytical first-order spin-flop/flip phase transition at $\pm H_{\mathrm{SF}}$, given by equation (2*a*) for $K/J < 1$ and $\pm J$ for $K/J > 1$. The white dashed lines are the second-order phase transition from the cAFM to the FM phase at $\pm H_{\mathrm{FM}}$, from equation (2*b*). Both fields are rescaled by $2J$. The gray dashed lines are the K/J values determined from experimental $H_{\mathrm{SF}}/H_{\mathrm{FM}}$ data for sample A at different pressures. (b) The effective K (solid triangles) and J (empty triangles) values as a function of temperature, extracted using equation (2) and experimental $H_{\mathrm{SF}}, H_{\mathrm{FM}}$. (c) The measured $H_{\mathrm{SF}}/H_{\mathrm{FM}}$ as a function of temperature.

not expected to depend on the temperature and this is confirmed by the experimental ratio shown in figure 3(c). From this data we have calculated the T-averaged ratio $K/J = 2/(1 + (H_{\mathrm{FM}}/H_{\mathrm{SF}})^2)$ and illustrate its evolution with pressure in the phase diagram in figure 3(a) with horizontal dashed lines. In short, the increasing width of both the AFM and cAFM phases on the H axis with increasing p can be explained within the two-sublattice model, where the interlayer AFM exchange J is substantially enhanced by pressure.

Finally, we discuss the curious hysteresis loops of the magnetoresistance curves in the AFM state of sample A, as well as our other devices, samples B, C and D which were approximately 33 nm, 43 nm and 10.3 nm thick, respectively. While sample A exhibits double hysteresis loops in the AFM phase, in the other samples we find a single hysteresis loop with finite remanence at $H = 0$ as shown in figure 4(a) from sample B. A remanent resistance in the AFM phase has previously been attributed to the coexistence of a ferromagnetic phase at room temperature

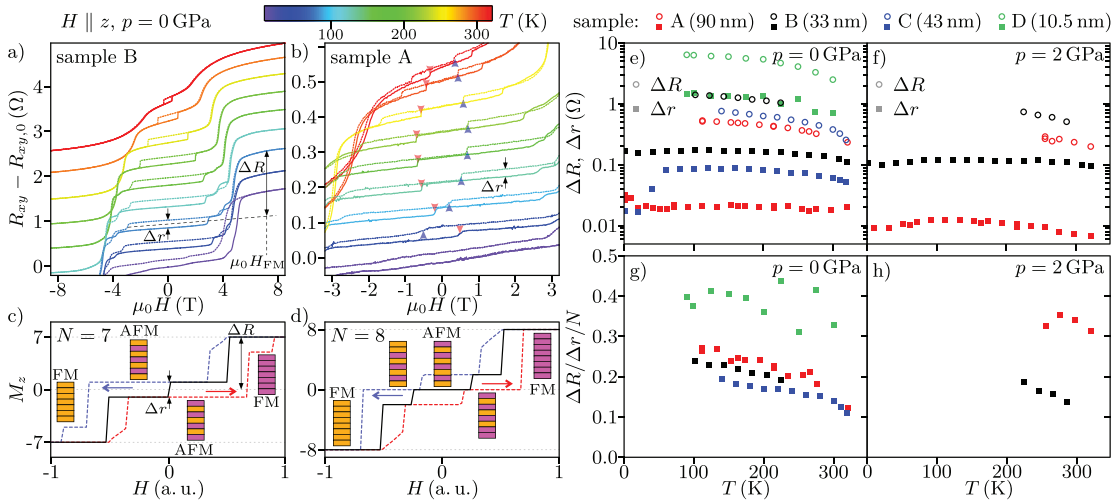

Figure 4. (a), (b) Fine structure of the anomalous Hall resistance in the AFM phase in samples B and A, respectively. The step and small loop heights $\Delta R, \Delta r$ are illustrated. In (b), red and blue triangles highlight the coercive fields closest to $H = 0$ of the double hysteresis loops. (c), (d) Simulations of the magnetization M_z for 7 and 8 layers following the global energy minimum of equation (4) (black lines), and simulations following the local energy minima for up and down sweeps (red and blue dashed lines). Stacks of rectangles indicate the magnetization M_{iz} of the individual layers in the global energy minimum at each H, with purple for positive and orange for negative. (e), (f) $\Delta R, \Delta r$ in multiple samples at 0 and 2 GPa, respectively. (g), (h) The ratio $\Delta R/\Delta r/N$ at 0 and 2 GPa.

[24]. In [23] a similar conclusion was drawn concerning even-layer samples from the increase of the remanent anomalous Hall resistance below 75 K. In the same reference, qualitative differences were observed between samples of even and odd layer number regarding the number of steps in R_{xy}, which were attributed to the role of surface layers and explained by modeling the magnetization of all layers, i.e. using the linear chain model.

Here we show that the linear chain model readily explains these observations without the use of a coexisting FM phase. The model [35, 36] uses the same parameters as equation (1), but treats the magnetization $\boldsymbol{M}_i$ of each layer (see figure 1(a)) individually:

$$f' = \frac{J}{2}\sum_{i=1}^{N-1} \boldsymbol{M}_i \cdot \boldsymbol{M}_{i+1} - \sum_{i=1}^{N}\left(\frac{K}{2}M_{iz}^2 + \boldsymbol{H}\cdot\boldsymbol{M}_i\right), \quad (4)$$

where N is the layer number. Each layer is coupled to two adjacent layers except at the surface, therefore $J/2$ is used. Surface layers are coupled to only one layer, which may lead to them switching at a different field than the bulk.

To illustrate the role of surface layers, we have calculated the global minimum of equation (4) with $N = 7$ and 8 layers. The results are discussed below, and are representative of odd and even layer systems within the model, with only quantitative differences between different N with the same parity (see SI). The net magnetization M_z in the global minimum for $N = 7, 8$ is shown by the black lines in figures 4(c),(d), respectively. In an odd-layer sample, M_z is always finite due to an uncompensated layer. There are two AFM states whose layer configurations are mirrored. In each AFM state, the layer directions M_{iz} are illustrated by colored rectangles with purple and orange for $M_{iz} > 0$ and $M_{iz} < 0$, respectively, similarly to figure 1(a). The system switches between them at $H = 0$ so that M_z remains aligned with H. This is shown by a step of the black line from -1 to $+1$ at $H = 0$ (figure 4(c)). However, in real samples such first order changes are hysteretic in general, because the system can remain in a state as long as it is an energy minimum, or until an external perturbation such as thermal excitations lead to relaxation into a lower-energy state. As a result, a hysteresis loop is expected to form around each predicted step of the black line. The $H = 0$ step should expand into a hysteresis loop as if for a FM, which matches the experiments on samples B (figure 4(a) as well as C, D (figures S3, S4 in the SI).

For $N = 8$, the calculated magnetization M_z in the global energy minimum is plotted in figure 4(d) by the black line. Here the AFM state is well defined around $H = 0$ with $M_z = 0$. In addition, plateaus of $M_z = \pm 2$ can be found between the AFM and FM states, which is characteristic for all even $N \geqslant 4$. Here, the surface layer that was antiparallel with H in the AFM state is now aligned with H and also its neighbor, as shown by the series of rectangles. Like for odd N, in reality a hysteresis loop is expected to form around each step, which is consistent with the double loop structure in sample A, replotted for comparison in figure 4(b).

As temperature decreases, the experimental data becomes more complex, as demonstrated by additional hysteresis loops in figures 1(c) and 4(a) around $\pm H_{SF}$. In sample A we also found a remanent AHE resistance, i.e. a finite difference at $H = 0$ between up- and down sweeps as can be seen in figure 4(b), similarly to [23] for even layers. However,

the evolution of the small loops with temperature makes it clear that the origin of the remanence, instead of a new FM state, is that the pair of small loops begins to overlap at low T, as displayed by the red and blue triangles. As a proof of concept, we have conducted theoretical calculations of the metastable states of the system. Now, instead of the global minimum, we always follow a local energy minimum until it becomes unstable. The red and blue dashed lines in figures 4(c) and (d) represent such calculated up- and down field sweeps, leading to a hysteresis with a complex shape. For an even layer number, this predicts a remanent magnetization around $H = 0$, leading to a finite AHE which is consistent with our low-T experimental findings in sample A.

Nevertheless, the parity of the layer number could not be confirmed due to the limited accuracy of atomic force microscopy measurements. Therefore, we conducted an analysis of the small loop height and the AFM-(cAFM)-FM step height in all samples to compare them to predictions by the chain model. For this we antisymmetrized the R_{xy} curves [34], and corrected them by a linear background attributed to the CHE, which we determined by fitting the regions near $H = 0$. We extracted the magnitude ΔR of AHE in the FM state at H_{FM} as shown in figure 4(a), to minimize systematic errors from a potentially nonlinear CHE. This step approximately corresponds to a magnetization change $\Delta M_z^{\Delta R} = N$ in thick samples. ΔR is shown in figures 4(e) and (f) at 0 and 2 GPa, and its temperature-dependence is comparable to that of $H_{\mathrm{SF}}(T)$. The height Δr of the small loop, estimated far from hysteresis overlaps (see figures 4(a) and (b)), corresponds to a $\Delta M_z^{\Delta r} = 2$ magnetization change and is also plotted in figures 4(e) and (f). In general, both ΔR and Δr slightly decrease with increasing pressure. They also decrease as the crystal thickness increases, which is consistent with the behavior of AHE in ferromagnetic sister compounds Fe_3GeTe_2 and Fe_3GaTe_2 [37–39].

We have calculated the ratio $\Delta R/\Delta r/N$, where the layer number N was estimated from the flake thickness, and plot it in figures 4(g) and (h). As discussed above, it is predicted to be $\Delta M_z^{\Delta R}/\Delta M_z^{\Delta r}/N = 0.5$, but according to our findings it is lower and depends on the temperature. These properties may originate, for example, in a H-nonlinear CHE that distorts ΔR, a different T-dependence of surface and bulk layer magnetizations (due to the presence or lack of a neighbor), or a different saturation state of the magnetizations as $\Delta r, \Delta R$ are read out at different fields, which the model does not account for. Nevertheless, the observed $\Delta R/\Delta r/N$ is comparable for several samples of various thicknesses, demonstrating a qualitative agreement with the chain model.

The magnetic properties of CFGT and its sister materials are extremely sensitive to the configuration of magnetic ions [24, 40, 41]. Therefore, the cause of the reduced ratio $\Delta R/\Delta r/N$ may be, in addition to those listed above, due to the effect of surface oxidation [42] on Δr. As Δr is related to AHE in the surface layers, we speculate that an increase in Δr may be produced in various ways, from a higher surface current density to having a different local magnetization or even a sign change of the local interlayer coupling J [43], which may be detectable via surface mapping techniques [44, 45]. A stronger surface spin-dependent scattering that enhances AHE is another possibility and may also contribute to the different T-dependence of $\Delta R, \Delta r$ in figures 4(e) and (f). Deviations may also be the result of inhomogeneities in the layer magnetization, stacking, etc.

5. Conclusions

We have studied the magnetic response in AFM $(Co_{0.5}Fe_{0.5})_5GeTe_2$ samples between 10 to 90 nm thickness via the anomalous Hall effect. We have clearly delineated the AFM, cAFM, and FM states and shown that, with pressure, the magnetic transition fields increase substantially and the cAFM state is stabilized. Although the anisotropy is practically unaffected, the interlayer AFM coupling J increases by approximately 50% when applying 2 GPa, demonstrating the sensitivity of magnetic parameters to the interlayer distance. In addition, we found that the small hysteresis loops within the AFM phase can be qualitatively explained by the behavior of the surface layers as predicted by the linear chain model. The analysis of the resistance steps to the FM state compared to those in the small loops is in line with this picture.

CFGT is the highest-Néel-temperature 2D antiferromagnet discovered to date [14]. We believe that our results shed light on the intriguing magnetic behavior of the bulk and the surface of CFGT crystals, and will contribute to the design of AFM components and interfaces in future spintronic devices.

Acknowledgments

This research was supported by the Ministry of Culture and Innovation and the National Research, Development and Innovation Office within the Quantum Information National Laboratory of Hungary (Grant No. 2022-2.1.1-NL-2022-00004 and UNKP-23-4-I-BME-36), by OTKA Grant No. K134437 and the NKKP STARTING Grant No. 150232. We acknowledge funding from the 2DSOTECH FlagERA network, the 2DSPIN-TECH

Flagship project, the Alexander von Humboldt Foundation, the European Research Council ERC project Twistrain, the TRILMAX Horizon Europe consortium (Grant No. 101159646), and COST Action CA 21144 superQUMAP. M. H. D. G. acknowledges funding from the Zernike Institute for Advanced Materials and the European Union, through grant ERC StG 2D-OPTOSPIN, Grant No. 101076932. H. S. and I. J. V. M. in Horizon Europe Project "2D Heterostructure Non-volatile Spin Memory Technology" (2DSPIN-TECH) are supported by UKRI grant number [10101734] (The University of Manchester).

The authors thank A. Márffy for his assistance with the pressure cell.

Samples were fabricated by B. Z., Z. K. K. and H. S. in Göteborg, Budapest and Manchester. Measurements were performed by T. P. and Z. K. K. in Budapest, and H. S. in Manchester. Analysis was carried out by T. P., M. L. M. and E. T. with the contribution of M. H. D. G. Research was guided by B. F., I. J. V. M., S. P. D., S. C., P. M. and E. T.

Data availability statement

All data that support the findings of this study are included within the article (and any supplementary files).

The data that support the findings of this study are available upon reasonable request from the authors.

Conflict of interest

The authors declare that no competing interests exist.

Statements

No human participants were included in this study besides the authors.

ORCID iDs

Tamás Prok 0000-0002-1240-6310
Zoltán Kovács-Krausz 0000-0001-5821-6195
Harvey Stanfield 0000-0001-7197-3983
Bing Zhao 0000-0002-5560-6750
Bálint Fülöp 0000-0001-6853-2642
Marcos H D Guimarães 0000-0002-8150-4379
Ivan J Vera-Marun 0000-0002-6347-580X
Saroj Prasad Dash 0000-0001-7931-4843
Szabolcs Csonka 0000-0003-0505-2806
Péter Makk 0000-0001-7637-4672
Endre Tóvári 0000-0002-0000-3805

References

[1] Baltz V, Manchon A, Tsoi M, Moriyama T, Ono T and Tserkovnyak Y 2018 *Rev. Mod. Phys.* **90** 15005
[2] Din A D, Amin O J, Wadley P and Edmonds K W 2024 *npj Spintron.* **2** 25
[3] Song T *et al* 2018 *Science* **360** 1214
[4] Klein D R *et al* 2018 *Science* **360** 1218
[5] Ningrum V P *et al* 2020 *Research* **2020** 1768918
[6] Elahi E *et al* 2022 *Comput. Mater. Sci.* **213** 111670
[7] Mi M, Xiao H, Yu L, Zhang Y, Wang Y, Cao Q and Wang Y 2023 *Mater. Today Nano* **24** 100408
[8] Jia Z *et al* 2025 *ACS Nano* **19** 9452
[9] Sierra J F, Fabian J, Kawakami R K, Roche S and Valenzuela S O 2021 *Nat. Nanotechnol.* **16** 856
[10] Yang H *et al* 2022 *Nature* **606** 663
[11] Song J, Chen J and Sun M 2023 *Mater. Today Electron.* **6** 100070
[12] Roche S, van Wees B, Garello K and Valenzuela S O 2024 *2D Mater.* **11** 43001
[13] Thapa A and Sharma B 2025 *Adv. Mater. Technol.* **10** e00133
[14] Zhao B, Ngaloy R, Pandey L, Bangar H, Dubey D P and Dash S P arXiv:2602.24046
[15] Fei Z *et al* 2018 *Nat. Mater.* **17** 778
[16] Deng Y *et al* 2018 *Nature* **563** 94
[17] Zhang G, Guo F, Wu H, Wen X, Yang L, Jin W, Zhang W and Chang H 2022 *Nat. Commun.* **13** 5067
[18] May A F, Ovchinnikov D, Zheng Q, Hermann R, Calder S, Huang B, Fei Z, Liu Y, Xu X and McGuire M A 2019 *ACS Nano* **13** 4436
[19] Zhao B *et al* 2023 *Adv. Mater.* **35** 2209113
[20] Tian C, Pan F, Xu S, Ai K, Xia T and Cheng P 2020 *Appl. Phys. Lett.* **116** 202402
[21] May A F, Du M-H, Cooper V R and McGuire M A 2020 *Phys. Rev. Mater.* **4** 74008
[22] Ngaloy R *et al* 2024 *ACS Nano* **18** 5240
[23] Lu L *et al* 2024 *Nano Lett.* **24** 5984
[24] Zhao B, Bainsla L, Ershadrad S, Zeng L, Ngaloy R, Svedlindh P, Olsson E, Sanyal B and Dash S P 2025 *Adv. Mater.* **37** 2502822
[25] Zhang H *et al* 2022 *Phys. Rev. Mater.* **6** 44403
[26] Zhang H *et al* 2024 *Adv. Mater.* **36** 2308555
[27] Fülöp B *et al* 2021 *J. Appl. Phys.* **130** 064303
[28] Li T *et al* 2019 *Nat. Mater.* **18** 1303
[29] Song T *et al* 2019 *Nat. Mater.* **18** 1298
[30] Nagaosa N, Sinova J, Onoda S, MacDonald A H and Ong N P 2010 *Rev. Mod. Phys.* **82** 1539
[31] Coey J M D 2010 *Magnetism and Magnetic Materials* (Cambridge University Press) pp 195–199
[32] Feder J and Pytte E 1968 *Phys. Rev.* **168** 640
[33] Aharoni A 2000 *An Introduction to the Theory of Ferromagnetism* (Oxford University Press)
[34] Márffy A *et al* 2026 *Nano Lett.* **26** 1782
[35] Wang Z, Gibertini M, Dumcenco D, Taniguchi T, Watanabe K, Giannini E and Morpurgo A F 2019 *Nat. Nanotechnol.* **14** 1116
[36] Ye C *et al* 2022 *ACS Nano* **16** 11876
[37] Tan C, Lee J, Jung S-G, Park T, Albarakati S, Partridge J, Field M R, McCulloch D G, Wang L and Lee C 2018 *Nat. Commun.* **9** 1554
[38] Roemer R, Liu C and Zou K 2020 *npj 2D Mater. Appl.* **4** 33
[39] Wang M, Lei B, Zhu K, Deng Y, Tian M, Xiang Z, Wu T and Chen X 2024 *npj 2D Mater. Appl.* **8** 22
[40] Ershadrad S, Ghosh S, Wang D, Kvashnin Y and Sanyal B 2022 *J. Phys. Chem. Lett.* **13** 4877
[41] Tyson T A, Amarasinghe S, Abeykoon A M M, Lalancette R, Du K, Fang X, Cheong S-W, Al-Mahboob A and Sadowski J T 2025 *2D Mater.* **12** 025021
[42] Li Y *et al* 2023 *ACS Appl. Nano Mater.* **6** 4390
[43] Kim D *et al* 2019 *Nanotechnology* **30** 245701
[44] Tschudin M A *et al* 2024 *Nat. Commun.* **15** 6005
[45] Pellet-Mary C *et al* 2025 *Nat. Commun.* **16** 9725